J. Coat. Technol. Res., **19** (3) 699–716, 2022
https://doi.org/10.1007/s11998-021-00579-6

REVIEW ARTICLE

A review on predictive tortuosity models for composite films in gas barrier applications

Alamin Idris, Adrian Muntean, Beko Mesic

Received: 14 April 2021 / Revised: 27 October 2021 / Accepted: 1 November 2021

Abstract Different types of impermeable fillers are usually incorporated into polymeric coating film to enhance the gas barrier properties. For instance, impermeable fillers are commonly used in barrier coating due to their larger surface, which in turn serve as barrier inclusions restricting the penetrant gas to diffuse through a longer tortuous pathway. Modeling gas transport in barrier coating can help determine the shelf-life of packaged food and reduce product development resources and time. In this paper, related tortuosity-based models corresponding to different filler geometries are outlined. This review emphasizes the emerging trends in modeling the tortuous pathway and the respective relative permeability model to predict the gas barrier performance in composite films used for barrier coating applications. We review models incorporating a range of factors, including different shapes, geometries, angular orientations, alignments, randomness in distribution, stacking, interspacing, and the polydispersity of fillers. The approaches employed to develop the tortuosity-based phenomenological models starting with simplified filler geometry and orientations to more complex morphological features of the composite films are elaborated.

Keywords Composites, Impermeable fillers, Oxygen barrier, Relative permeability, Tortuosity

A. Idris (✉), B. Mesic
Department of Engineering and Chemical Sciences, Karlstad University, 651 88 Karlstad, Sweden
e-mail: alamino97@yahoo.comalamin.abdulgadir@kau.se

A. Muntean
Department of Mathematics and Computer Science, Karlstad University, 651 88 Karlstad, Sweden

Introduction

The search for effective gas barrier materials has been extensively explored for various applications such as food packaging, biomedical application, energy, protective coating, etc.[1, 2] Over the past decades, polymeric materials have received significant attention due to their functionality, low cost, lightweight, easy processing, and appreciable mechanical properties such as excellent tensile strength and high flexibility.[3, 4] The polymeric materials commonly used in packaging applications are polypropylene (PP), polystyrene (PS), polyethylene terephthalate (PET), polyvinyl alcohol (PVA), ethylene vinyl alcohol (EVA), polylactic acid (PLA), polyvinyl chloride (PVC), and polyethylene (PE). These polymers have high versatility, and their barrier properties are one of the most important factors in food packaging applications. In addition to that, the sustainability factor, where sustainable packaging solutions can provide a significant contribution to the food source handling, where challenges related to waste are pertinent.[5]

In general, the packages made from polymer films are permeable at different degrees to small molecules like gases, water vapor, and other low molecular weight volatile compounds present in the food. Because of the packaging material properties, the transfer of these molecules ranges from a low, medium, to high, as reflected in low, medium, and high barriers, respectively.[6] PVA, EVA, PLA, and starches belong to sustainable packaging materials that are attractive for packaging applications where a good oxygen barrier is required. These four polymeric materials are usually used in dispersions applied onto cellulose fiber-based substrates to provide versatile, sustainable packaging solutions in many applications. The oxygen barrier is a vital barrier property when fatty foodstuff is packaged.[7, 8]

The barrier properties of the polymer film can be significantly enhanced by the incorporation of impermeable inorganic materials into the polymeric film. The enhancement can be described as the combination of two phenomena, i.e., a reduced diffusion area and prolonged diffusion time.[9] In other words:

- The incorporation of impermeable lamellar fillers in permeable polymer matrix results in a reduced available diffusion area.
- The diffusion of gas molecules occurs through a tortuous pathway around the impermeable filler, prolonging the gas diffusion pathways.

Therefore, a significant reduction in permeability is generally observed in polymer–inorganic composite films. For this reason, extensive experimental research works have been conducted worldwide to investigate the role of the inorganic fillers in composite polymer films targeting improved barrier properties. The different experimental results reported are based on the filler and polymer types and the dispersion of the fillers in the polymer matrix. Generally, the gas barrier performance of the polymer composite films is characterized by three main factors: (1) filler properties such as shape factor, content, aspect ratio, dispersity, volume fraction, filler adsorption, and activity/resistance to gas diffusion, (2) the properties of a core polymer material such as the intrinsic barrier property or the permeability, crystallinity, and (3) the dispersion quality in the composite film such as the filler distribution, orientation, exfoliation, intercalation, agglomeration, interfacial formations, etc.[10] It is worth mentioning that the successful development of polymer composite film should exhibit a defect-free surface, homogenous dispersion, and completely exfoliated layers of the fillers in the polymer matrix.

Various impermeable inorganic minerals have been utilized as fillers in a polymer matrix, forming a composite system to achieve enhanced barrier properties. Among the commonly used fillers are mostly clay minerals such as kaolinite, bentonite, montmorillonite, cloisite, vermiculite, mica, halloysite, and talc,[11–14] and other forms of domains such as layered silicates,[15, 16] graphene oxide,[17] cellulose nanocrystals,[18] and spherical silica.[19, 20] Besides being environmentally friendly materials, these fillers are usually preferred for their desirable geometry, such as platelets, rectangular, hexagonal, octagonal flakes, ribbons, discs, spherical, and cylindrical shapes of infinite length. Such geometries of impermeable fillers serve as barrier domains, enhancing the oxygen barrier performance of the composite system.

This work aims to review the various tortuosity models developed progressively by the scientific community to predict the permeability of the oxygen through composite materials systems consisting of polymer (both thermally processed and dispersible) and impermeable fillers in the interest of barrier applications. The article initially covers the tortuosity models developed for simpler geometries of fillers, i.e., regular dispersion, uniform sizes (monodispersed), and parallelly oriented or aligned particles or flakes. Further, it also explores the different modifications introduced to account for the added complexities in system morphologies, such as variations in filler geometries, polydispersity, filler dispersions, shapes, orientations, and irregularities such as stacking, agglomeration, and intercalations. Furthermore, comparisons of selected model predictions are also presented.

Theoretical background

Generally, there are two fundamental gas transport mechanisms in polymer systems: the solution-diffusion and pore-diffusion mechanisms. These mechanisms were first proposed by Thomas Graham more than a century ago.[21, 22] For dense polymer systems such as barrier films and membranes, the solution-diffusion mechanism is the most popular and relevant description for the gas transport model, usually expressed in terms of permeability.[21] At a given temperature, the gas permeability or the transport of gas molecules in a homogeneous polymer system is affected by three main processes: (1) the gas molecules are first absorbed on the upstream surface of the polymer film (i.e., high chemical potential side), (2) then they diffuse across the thickness of the film and (3) finally get desorbed on the downstream side of the polymer film (i.e., low chemical potential side) (see Fig. 1).[23, 24] The absorption and desorption steps occur very fast as compared to the diffusion step, and thus, the diffusion is a rate-

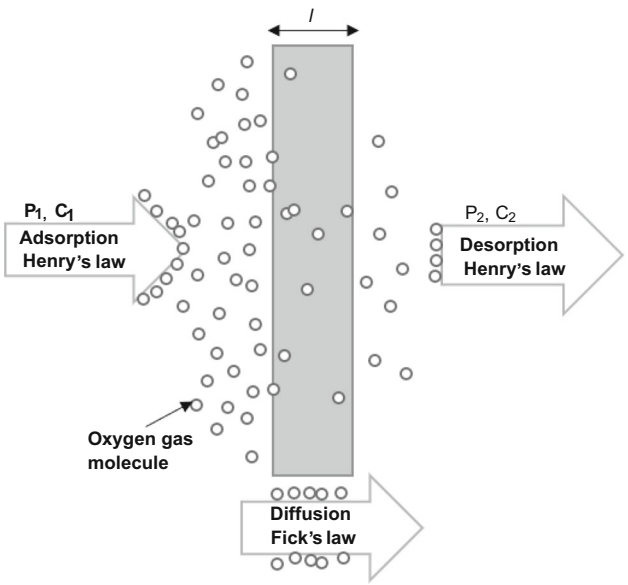

Fig. 1: Schematic of solution-diffusion mechanism in a polymeric coating film

limiting step in mass transfer through the film. The gas diffusion across the cross section of the film usually takes place under the influence of the driving force. This driving force is typically a pressure gradient corresponding to the chemical potential difference across the film sides.[25]

According to the Fickian transport mechanism, the time required for a gas molecule to reach the equilibrium state is shorter than the characteristic diffusion time. Both the diffusivity and solubility parameters are dependent on the properties of the polymer material and the penetrating gas. Thus, the gas permeability (P) in polymer systems is defined as the product of two factors, i.e., the gas solubility (S) and the gas diffusivity (D), which is expressed as follows:

$$P = DS. \tag{1}$$

The gas solubility is a thermodynamic parameter associated with the gas molecule–polymer interaction (i.e., penetrant affinity), the polymer fractional free volume, and the gas condensability and polarity. According to Henry's law, gas solubility is described as the ratio of gas concentration dissolved in polymer to the gas pressure, whereas the gas diffusivity is a kinetic parameter associated with the free volume and the molecular mobility in the polymer matrix.

For gas transport through polymeric systems, diffusion is the most dominant mechanism. According to Fick's law, diffusivity is described as the proportionality constant among the diffusive flux and the concentration gradient. For one dimensional diffusion, Fick's first law can be expressed as:

$$J = -D\frac{\partial C}{\partial x}, \tag{2}$$

where J and ∂C/∂x are the diffusive flux and the concentration gradient of the solute gas, respectively. For a known thickness of the polymeric film l, assuming the steady-state conditions and constant diffusivity, the penetrating gas flux can be approximated as:

$$J = -D\frac{\Delta C}{l}, \tag{3}$$

thus, the gas permeability in pure polymer films in terms of the diffusive flux and pressure gradient can be obtained as follows:

$$P = \frac{\mathrm{Jl}}{\Delta P} = \frac{Q_{\mathrm{STP}}l}{A\Delta P}, \tag{4}$$

where Q_{STP} is the gas flow rate at standard temperature and pressure (cm^3 (STP)/s), A is the effective film area (cm^2). ΔP is the pressure gradient across the film sides (cm.Hg). Equations (1)–(4) are commonly employed to calculate the gas permeability in a pure polymer film. However, upon adding impermeable fillers, i.e., a dispersed phase, in the polymer matrix, the permeability values change significantly due to the change in the available diffusion area as well as the diffusion pathways. To account for the fillers' impact on the gas transport properties, several models have been proposed in the literature correlating the diffusion of the penetrant gas with the characteristic features of the systems. Among the various characteristic parameters, the geometrical parameters of fillers such as shape, size, diameter, thickness, distribution, etc., which led to the tortuous pathway of gas transport, have been considered in detail.

The solubility S is assumed to be independent of the filler's morphological features in such composites, which is given as[26]:

$$S = S_o(1 - \phi_d), \tag{5}$$

where S_o is the solubility in pure polymer, and φ_d is the volume fraction of the dispersed filler platelet. If platelets behave as an entirely impermeable barrier, then the diffusing gas molecules will take longer tortuous diffusional pathways across the film thickness. Thus, the diffusion coefficient is affected by the tortuosity factor τ. Therefore, the commonly agreed dependence of diffusivity D is as follows:

$$D = \frac{D_o}{\tau}, \tag{6}$$

where D_o is the gas diffusivity in a pure polymer film. The relative permeability is directly related to the volume fractions of either polymer or the dispersed phase and the tortuosity factor. Thus, combining equations (1), (5) and (6). The relative permeability equation can be calculated as [27, 28]:

$$\frac{P}{P_o} = \frac{\phi_p}{\tau} = \frac{(1 - \phi_d)}{\tau}, \tag{7}$$

where P and P_o denote to the permeability of the polymer–inorganic composite film and pure polymer film, respectively. φ_p is the volume fraction of the polymer. τ is the tortuosity factor defined as a ratio of the distance a gas molecule must travel to get across the film thickness to the thickness of the composite film.[29] The tortuosity factor is dependent on the filler's aspect ratio, shape, dispersion quality, and the orientation of the inorganic platelets in the polymer matrix.

Analytical models for tortuosity

Numerous analytical models for tortuosity have been developed to predict the barrier performance of composite material films. These studies considered various transport contributions, typically related to the composite system's tortuous pathway resistance, de-

fined in a simplified way. Our study presents the different models progressively developed, especially for composite systems with microscale structure features in mind, to determine the barrier properties of polymer–filler composite films. Various aspects, such as filler geometry and orientation, filler-polymer matrix interphase, and filler layer agglomeration, are considered when modeling the composite film systems.

Effects of filler shapes

Diffusion of gaseous molecules through a composite film containing a dispersed impermeable filler is a classical transport phenomena problem. The first example treating such phenomena goes back to Maxwell, often known as Maxwell's theory.[30] The theory considers a regular array of impermeable spherical fillers with a perfect filler–polymer matrix contact (without any interfacial defects) (see Fig. 2). The model can predict the relative permeability in the dilute dispersion of the fillers in the polymer matrix. The Maxwell model and the tortuosity factor are given as follows[30]:

$$\frac{P}{P_o} = \frac{1-\phi_d}{(1+\phi_d/2)}. \tag{8}$$

According to equation (7), the denominator in the Maxwell model [equation (8)] corresponds to the choice of the tortuous pathway. Thus, the tortuosity expression can be conveniently described as:

$$\tau = 1 + (1/2)\phi_d. \tag{9}$$

It should be noted that the Maxwell model is applied for filler concentrations less than 20% ($\varphi_d < 0.2$). Under this condition, spheres can cause a relatively low impact on the barrier properties of composite films. For instance, the relative gas permeabilities reduce to 0.91, 0.83, and 0.75, if the filler concentrations are 6%, 12%, and 18%, respectively.

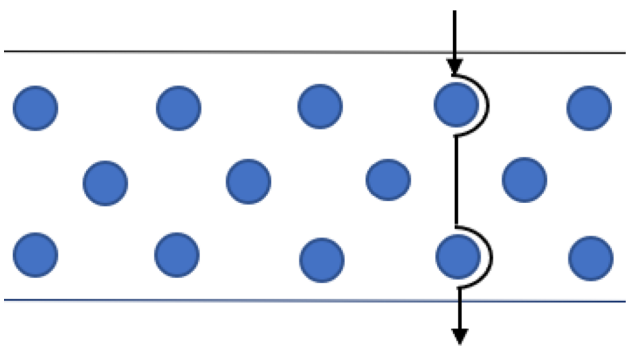

Fig. 2: Schematic diagram for a diffusing gas in a composite system with spherical filler shapes[30, 31]

Similarly, Rayleigh[32] reported a simpler tortuosity-based expression for the prediction of relative permeability in films containing periodically arrayed cylinders with infinite length and oriented parallel to the film surface. In this case, we have:

$$\frac{P}{P_o} = \frac{1-\phi_d}{1+\phi_d}, \tag{10}$$

$$\tau = 1 + \phi_d. \tag{11}$$

The limitation of Rayleigh model [equation (10)] is similar to that Maxwell Model [equation (8)], which is only valid for low concentration of the fillers. However, it is clear that both the models are independent of the size of the fillers but varies with the filler loading.

Bruggeman[33] developed an important model describing the effects of additional fillers to a system of composite films with dilute suspensions for randomly dispersed spherical fillers. The model was then modified for nonporous-impermeable fillers.[34, 35] The expression for the relative permeability is described as:

$$\frac{P}{P_o} = (1-\phi_d)^{3/2}. \tag{12}$$

The tortuosity expression used in Bruggeman model is expressed as follows:

$$\tau = (1-\phi_d)^{-1/2}. \tag{13}$$

The Bruggeman model is simply a modification to the Maxwell model for a larger range of φ_d with a random dispersion. However, both models exhibit similar limitations as the filler's shape, size distribution, and dispersions are not considered in the model formulation.

Later, Maxwell–Wagner–Sillars (MWS) model was developed as an extension to the original Maxwell model to account for the effects of different shapes of the dispersed filler by introducing a shape factor n ($0 < n < 1$) in dilute dispersion.[36] The shape factor value for prolate ellipsoids fillers varies $0 \le n \le 1/3$, and for oblate ellipsoids fillers, the value changes within the range of $1/3 \le n \le 1$. For more details on the shape factor values, see the literature.[37, 38] The original MWS model expression can be simplified and reads as:

$$\frac{P}{P_o} = \frac{(1-n)(1-\phi_d)}{1-n+n\phi_d}. \tag{14}$$

For spherical fillers, i.e., when $n = 1/3$, equation (14) reduces to Maxwell model equation (8). Comparing equation (14) with equation (7), the tortuosity expression in the MWS model reads as follows:

$$\tau = 1 + \frac{n}{(1-n)}\phi_d. \tag{15}$$

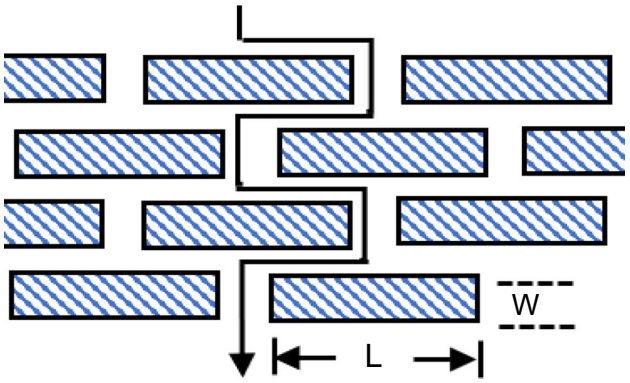

Fig. 3: Schematic diagram indicating a tortuous path of a diffusing molecule assumed in Nielsen model[39]

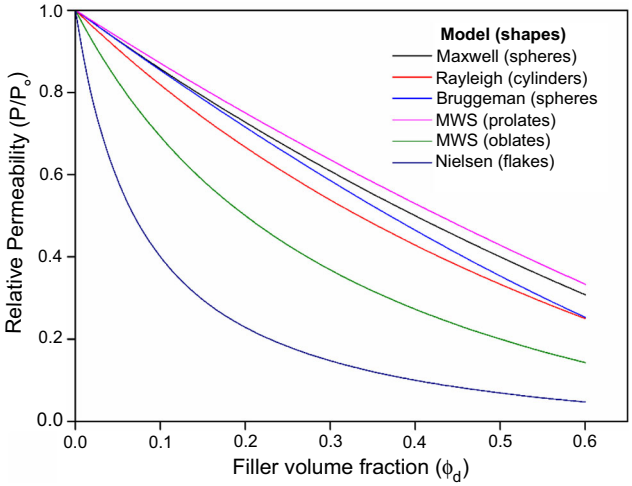

Fig. 4: Comparison of different filler shapes considered in various phenomenological models: Shape factors of 0.25 and 0.75 are considered for prolates and oblates in MWS model, respectively, and an aspect ratio of 25 assumed in Nielsen model

Effects of filler alignments

The incorporation of impermeable fillers deters the diffusion pathway restricting the gas molecules to diffuse through the amorphous regions of the polymer film. Tortuous pathways are then followed depending on the distribution of the fillers in the polymer matrix. In 1967, Nielsen[39] introduced the first tortuosity model to predict the permeability in composites films consisting of polymer and clay filler. A single layer of circular or rectangular clay mineral platelet was assumed to be in an even/regular dispersion with complete exfoliation and perpendicularly aligned to the direction of diffusion.

According to Nielsen, the tortuous pathway is assumed to be the longest distance traveled by a diffusing gas molecule under the influence of chemical potential difference across the film thickness. For the given geometry of the system shown in Fig. 3, the tortuosity equation is given by:

$$\tau = 1 + (L/2W)\phi_d, \tag{16}$$

where L and W are the length and thickness of the filler platelets. Combining equations (7) and (16), the relative permeability is expressed as:

$$\frac{P}{P_o} = \frac{(1-\phi_d)}{1+(L/2W)\phi_d}. \tag{17}$$

The ratio L/W is often known as the aspect ratio (α). This is typically used as a characteristic filler's geometrical parameter to describe the reduction in gas flow across the composite film. The model is a function of filler volume fraction and the aspect ratio. To demonstrate the effects of fillers basic geometric shapes on the barrier performances as proposed in the phenomenological models developed, the models are compared as presented in Fig. 4. The plot shows the comparison of Maxwell [equation (8)], Rayleigh [equation (10)], Bruggeman [equation (12)], MWS [equation (14)], and Nielsen [equation (17)] models relative permeability predictions as a function of filler concentrations. It should be noted that some models such as Maxwell and Rayleigh models may not be valid for filler concentrations (φ_d>0.2). Simple illustration on the effects of filler shapes on the relative permeabilities is shown in Fig. 4.

According to Fig. 4, it can be noted that spheres and cylinders do not exhibit a major impact on the barrier performance of the composite system. For instance, with a 10% volume fraction of fillers (φ_d=0.1), the permeability of the composite film with spherical fillers reduces to $0.86P_o$ (Maxwell model) and $0.85P_o$ (Bruggeman model). For cylinders 18% reduction (i.e., $0.82P_o$) (Rayleigh model), and for prolate and oblate ellipsoids (MWS model) $0.87P_o$ and $0.69P_o$, respectively. Furthermore, for rectangular flakes with an aspect ratio of 25, the predicted permeability of the composite is reduced by 60% ($0.4P_o$) as predicted using Nielsen model. However, if fillers with cube shapes are used for which its aspect ratio is unity, the Nielsen model prediction results in identical values as the Maxwell model. Therefore, it clear that rectangular flakes with infinite length have a more significant effect than the impermeable fillers with sphere, cylinder, ellipsoid, and cube shapes. Moreover, the results for layers of flakes are significantly different since flakes cannot be defined with a single dimension like spheres; for instance, width and thickness are required a ribbon-shaped flake. In addition to that, the alignment of the flakes is crucial to achieve the desirable barrier properties.[40]

Using Nielsen model, the predicted relative permeability of the composite film decreases with the increase in the parameters φ_d and α, as shown in

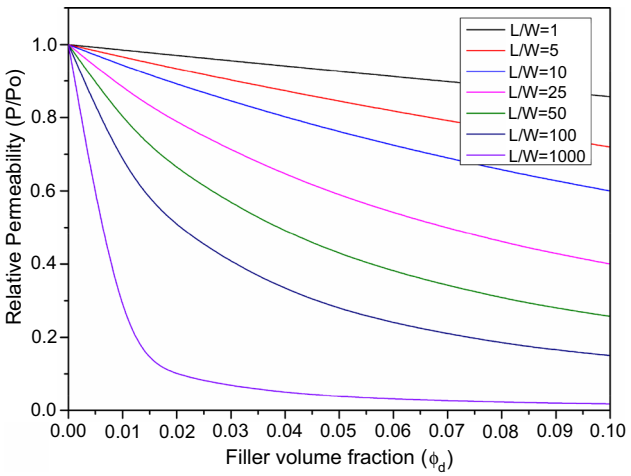

Fig. 5: Prediction of relative permeability using Nielsen model as a function of filler concentration with perpendicular alignment and aspect ratio

Fig. 5. According to the Nielsen model, for perpendicularly aligned filler, the aspect ratio should be high to achieve an appreciable gas barrier property. Fillers with a high aspect ratio could be found in clay minerals such as montmorillonite, laponite, bentonite, kaolinite, vermiculite, graphene, and synthetic mica. They exist in stacked layers with approximately 10–2000 nm in length and 1 nm thickness.[41] Several experimental results dealing with polymer–clay nanocomposite films revealed a filler aspect ratio as high as 10–2000 resulted in significant barrier enhancements.[42–44] However, increased filler content tends to agglomerate resulting in filler stacking and intercalation. Hence, the model validity is limited to 10% ($\varphi_d \leq 0.1$), or in other words, the model is applicable for dilute systems ($\alpha.\ \varphi_d \ll 1$). Fig. 5 shows that the barrier performance of composite film improves significantly with the increase of aspect ratio α. Significant enhancement can be observed in the barrier performance of composites even at low volume fractions of clay layers ($\varphi_d = 0.0015$) and higher values of aspect ratio ($\alpha \geq 1000$). For lower values of aspect ratio ($\alpha \geq 50$), Nielsen's model predicts almost a linear barrier enhancement with an increase in the volume fractions of clay φ_d. It can also be noted that the percentage of reduction in the relative permeability is found to be higher for fillers with higher aspect ratio than those with lower aspect ratio values. For instance, for $\varphi_d = 0.05$, the percentage reduction in relative permeabilities are 17.7%, 69.7% and 95.9% for aspect ratios of 10, 100 and 1000, respectively.

Few authors have modified Nielsen model to predict the relative permeability in composites with random dispersed inorganic flakes.[45] The modification appears to account for 30% randomness of the dispersed filler in the composite film. The modified Nielsen's model and the corresponding tortuosity expression for this case are given as follows:

$$\frac{P}{P_o} = \frac{(1-\phi_d)}{1+(1/3)(L/2W)\phi_d}, \tag{18}$$

$$\tau = 1 + \left(\frac{1}{3}\right)\left(\frac{L}{2W}\right)\phi_d. \tag{19}$$

Following Nielsen model, various models were developed and further modified to reflect the morphological features of the composite films. In addition to the consideration of the fillers, which are impermeable to the diffusing gas, various studies considered different shapes such as ribbons, discs, cylinders, etc. Most of the models considered a dilute or semi-dilute regime of the fillers with the intention to minimize the possibility of overlapping. Besides that, several investigations focused on the perpendicular alignment of the fillers to the diffusing gas. With this perspective, Cussler et al.[9] developed a predictive tortuosity model for different arrays of dispersed ribbons of infinite length. Both regular and random arrays of perpendicularly oriented platelets were considered during the model development, as shown in Fig. 6.

Although the prediction of Nielsen's model is rather accurate for low volume fractions of clay φ_d, however, it was considered as invalid by Cussler et al.[9] for low volume fraction of clay fillers when the fillers overlap or intercalate among each other (i.e., $\varphi_d \ll 1$ and $\alpha\ \varphi_d >> 1$). The aspect ratio is used as a measure of flake shape defined as α=d/a, where d and a are the thickness and width of the flake. In such morphological features, Cussler et al.[9] provided a different tortuosity relationship which can be employed for composite films containing perpendicularly oriented clay layers to the diffusion direction, as shown in Fig. 6a. Here, it holds:

$$\frac{P}{P_o} = \left(1 + \frac{\alpha^2\phi_d^2}{1-\phi_d}\right)^{-1}, \tag{20}$$

$$\tau = 1 + \frac{\alpha^2\phi_d^2}{1-\phi_d}. \tag{21}$$

The above equation [equation (20)] can be verified experimentally, especially for barrier films employed in packaging applications. For instance, Huang et al.[46] reported high barrier nanocomposite films composed of graphene oxide nanosheet filler and poly(vinyl alcohol), with a reduction in oxygen permeability of 98% at a low filler concentration of 0.72%. The reported experimental results are in good agreement with the predicted results. Their findings reveal that the nanosheet filler features are similar to those described in Cussler model, which is aligned parallel to the film surface.

Generally, it is unlikely to produce a composite film with clay flakes distributed in a regular array or with equal intervals due to the differences in material properties such as differences in flakes sizes, particle–

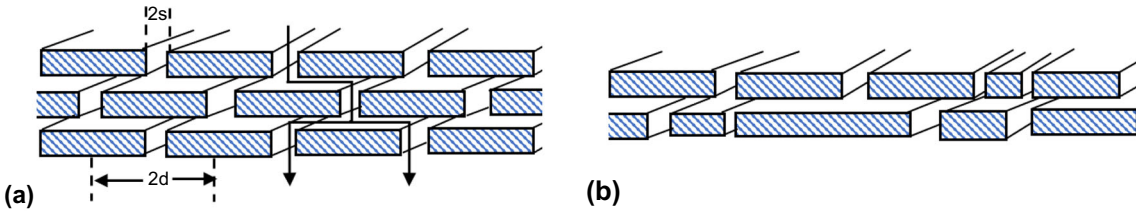

Fig. 6: Schematic diagram of diffusing gas in slits considered in Cussler model: (a) regular array and (b) random array[9]

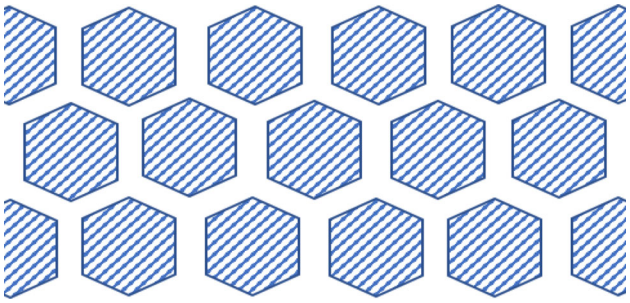

Fig. 7: Hexagonal-shaped ribbon-like fillers in a composite system

polymer interactions, etc. Thus, the flakes usually appear randomly distributed across the film. Therefore, two possible cases of alignments are considered for further modification of the model [equation (21)]. Equal probability of flake layers appears with alignment–misalignments and randomly misalignment of hexagonal flake layers. For the aligned and misaligned flake layers with an equal probability of occurrence, the tortuosity equation proposed is given as follows:

$$\tau = 1 + \frac{\alpha^2 \phi_d^2}{2(1-\phi_d)}. \tag{22}$$

For hexagonal flake shapes arranged in regular parallel arrays with a random misalignment of flake layers, it holds[47]:

$$\tau = 1 + \frac{2\alpha^2 \phi_d^2}{27(1-\phi_d)}. \tag{23}$$

Moggridge et al.[48] examined the tortuosity expression equation (23) for hexagonal shaped and aligned ribbon-like flakes in an attempt to predict the corresponding relative permeability for a composite system composed of polycarbonate polymer and mica filler (see Fig. 7). They obtained:

$$\frac{P}{P_o} = \left(1 + \frac{2}{27}\frac{\alpha^2 \phi_d^2}{(1-\phi_d)}\right)^{-1}. \tag{24}$$

In particular, the authors reported a good agreement of predicted results with experimental results using SEM measured aspect ratios α of 65 and 170 for ribbons and hexagons fillers, respectively.[48]

The tortuosity expressions [equations (22) and (23)] are, in fact, the special cases of Cussler model. They can be generalized by introducing factor ξ which depends on the shape of the flake filler, and on the dispersion or alignment within the polymer matrix. In this sense, a generalized tortuosity model can be:

$$\tau = 1 + \xi \frac{(\alpha \phi_d)^2}{1-\phi_d}. \tag{25}$$

In equation (25), one uses ξ=1 for ribbons or flakes dispersed in a regular array as shown in Fig. 6a, ξ = 1/2 for aligned-misaligned flakes with equal likelihood of occurrence,[47] and ξ = 2/27 for hexagonal flake layers with random misalignment.[48] Furthermore, the generalized tortuosity model pointed out in [equation (25)] was also extended to nanocomposites containing nanoplatelets. In such a case, one takes ξ = 1/4 for perpendicularly oriented nanoplatelets to the diffusion direction, ξ = 1/8 for two courses of nanoplatelets with equal probability of alignment and misalignment, and ξ = 1/54 for successive layers of randomly aligned hexagonal nanoplatelets.[49]

Effects of filler spacing

According to the findings reported by Wakeham and Mason,[50] there exists a resistance encountered to gas molecules to diffuse through multiperforated laminae. This resistance to diffusion is somehow similar to that diffusion resistance attributed to the need for the diffusing gas to enter into the slit constriction and diffuse through the depth or length of the slit in flake-filled composite films. Hence, Cussler et al.[9] considered such diffusion resistance and extended their model for a composite system of rectangular flake platelets of uniform sizes and perfectly dispersed with equal intervals (see Fig. 8). The idea was to introduce a slit aspect ratio (σ) or sometimes also called a slit factor, which is defined as the ratio of slit dimension (distance between to subsequent flake in the same layer) to the thickness of the flake ($\sigma = s/a$). The factor describes the resistance for diffusing penetrant gas molecules to diffuse through the slit/channel (space between two adjacent flakes and the contribution of the slit depth).

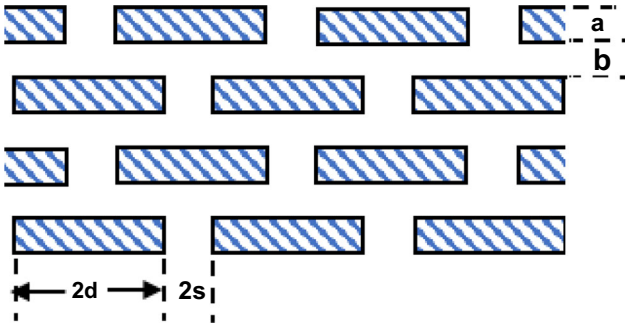

Fig. 8: Rectangular flake platelets with uniform size and perfectly dispersed with equal intervals

The adapted expression for the tortuosity, including the contribution of the slit space and depth (i.e., slit aspect ratio σ), can be expressed as:

$$\tau = 1 + \frac{\alpha\phi_d}{\sigma} + \frac{\alpha^2\phi_d^2}{1-\phi_d}. \tag{26}$$

Interestingly, equation (26) can be verified experimentally. For instance, this has been done by Eitzmann et al.[51] to validate the model using composite films composing of silicone-polycarbonate and oriented mica flakes. It has been reported that if $\sigma\alpha \ll 1$, then wiggles are dominant in the composite film, which seems to be the main contribution to the increased resistance in barrier films with flake-filled fillers.[51, 52] Thus, equation (26) reduces to equation (21). A good agreement was reported with such a case of dominant wiggles. However, if $\sigma\alpha >> 1$, then equation (26) reduces to:

$$\tau = 1 + \frac{\alpha\phi_d}{\sigma}. \tag{27}$$

According to the expression [equation (27)], it appears that only the wiggles can limit the diffusion of gas molecules but not the platelets. Equations (21) and (27) provide the required results for the 2D model presented in Fig. 8. They can give the change in permeability caused by the fillers as a function of the aspect ratio α, slit aspect ratio σ, and volume fraction of flake platelets φ_d. These parameters need to be varied to cross-verify the prediction precision against experimental results.

Using a conformal mapping, Aris[53, 54] formulated his analytical tortuosity model for a composite film with nanoplatelet filler. Following Aris's results, Falla et al.[55] proposed a slightly different tortuosity model for a similar system to what is presented in Fig. 8. This model considers the flakes' geometric dimensions, i.e., width $2d$, thickness a, flake layer spacing b, and the slit space $2s$ (the gap between two flakes). The proposed model reports:

$$\tau = 1 + \frac{\alpha^2\phi_d^2}{(1-\phi_d)} + \frac{\alpha\phi_d}{\sigma} + \frac{4\alpha\phi_d}{\pi(1-\phi_d)}\ln\left(\frac{\pi\alpha^2\phi_d}{\sigma(1-\phi_d)}\right). \tag{28}$$

On the right-hand side of equation (28), the first term "1" corresponds to the limit without flakes (i.e., when $\varphi_d = 0$). The second term is proportional to α^2 and refers to the diffusion resistance via the tortuous path around the flake, often known as wiggles. Both α and φ_d are squared to capture the prolonged diffusion distance and the decreased cross-sectional area among the flakes. The third term corresponds to the diffusion resistance induced by the slit, i.e., the constriction of the slit between platelets. These first three terms are common to the established tortuosity expression provided by Cussler model [equation (21)]. The fourth term is the newly introduced necking effect or constriction resistance for the gas molecules encountered entering in and exiting out of the narrow-slit space, i.e., the resistance for a diffusing molecule to find the slit.[56]

Again, following the findings reported by Wakeham and Mason,[50] Falla et al.[55] reported a similar model [equation (28)] with a modified fourth term, which is shown in the following tortuosity equation:

$$\tau = 1 + \frac{\alpha^2\phi_d^2}{(1-\phi_d)} + \frac{\alpha\phi_d}{\sigma} + 2(1-\phi_d)\ln\left(\frac{(1-\phi_d)}{2\sigma\phi_d}\right). \tag{29}$$

The difference in the fourth terms of equations (28) and (29) (i.e., the necking effect term) is that the latter is independent of the aspect ratio σ. These two relations are widely used to compare the predicted barrier performance with experimental results. These two expressions in equations (28) and (29) result in different predictions, particularly if the slit aspect ratio σ and the aspect ratio α are large. For instance, the necking term in equation (28) can have a significant effect, whereas equation (29) predicts either a small effect or even a wrong one (i.e., a negative value provided that the value within the logarithm is less than 1).[57]

Minelli et al.[58] suggested a different analytical model for the prediction of barrier performance in an ordered composite system. They introduced a new formulation for estimating gas transport properties in simplistic nanocomposite geometries. They claimed that their model correctly describes the enhanced barrier performance for various ranges of filler platelet loadings and dimensions. The model can be effectively used to extract insights on gas permeability in actual composite systems. The proposed tortuosity expression for their model is shown below:

$$\tau = \frac{\alpha\phi_d}{\sigma}\left(1+\frac{\sigma}{\alpha}\right)^2 + \frac{\alpha^2\phi_d^2(1+\sigma/\alpha)^4}{1-\phi_d(1+\sigma/\alpha)} + \frac{4\alpha\phi_d}{\pi}\left(1+\frac{\sigma}{\alpha}\right)^2 \ln\left(\frac{(1-\phi_d)(1+\sigma/\alpha)}{\sigma\phi_d(1+\sigma/\alpha)(\pi/2)}\right). \quad (30)$$

The first term of equation (30) corresponds to the resistance of mass transport attributed due to the tortuous path, whereas the second and third terms correspond to the tortuous path followed by the diffusing gas molecules.

Figure 9 shows the comparison of four different models outcome, i.e., Falla–Aris model [equation (28)], Falla–Wakeham and Mason model [equation (29)], Minelli model [equation (30)], and Cussler model [equation (21)]. The demonstration is made for two different aspect ratios of the filler (α =1000 and 500), and the slit aspect ratio σ is assumed to be 15. The outcome of the models' predictions for filler loadings above 1.5% and 3.5% is almost identical for filler aspect ratios of 1000 and 500, respectively. However, for dilute filler loadings, the models predictions exhibited different outcomes. To give an example, Falla–Wakeham and Mason model [equation (29)] overestimates the barrier enhancement in dilute regimes.

Effects of random arrangement of fillers

In another modeling approach, Minelli et al.[59] have extended the fundamental work assessing the effects of tortuosity reported by Aris. The extended model aims to describe barrier enhancement in random nanocomposite systems better. With the use FEM techniques used to characterize the geometry of the fillers, the model investigates the resistance to diffusion through the slit or the gap between subsequent flakes. The tortuosity model recognizes two regimes which are described as a function of aspect ratio α and the filler concentration φ_d :

$$\tau = \begin{cases} \left(\frac{\phi_d}{2\alpha}(\alpha+2)^2 + \frac{\phi_d^2(\alpha+2)^4}{4[\alpha^2-\alpha\phi_d(\alpha+2)]} + \frac{2}{\pi}(\alpha+2)^2\ln\left[\frac{2}{\pi}\left(\frac{\alpha}{\phi_d(\alpha+2)}-1\right)\right]\right)^{-1}, r \le 1, \\ \left(1+\frac{\phi_d}{2}(\alpha+2)+\frac{2\phi_d}{\pi\alpha}(\alpha+2)^2\ln\left[\frac{1}{\pi}(\alpha+2)\right]\right)^{-1}, r > 1, \end{cases} \quad (31)$$

where r is the control parameter defined as follows:

$$r = \frac{2(\alpha-\phi_d(\alpha+2))}{\phi_d(\alpha+2)^2}. \quad (32)$$

Lape et al.[61] considered rectangular platelets of identical aspect ratio (i.e., monodispersed flakes) with random arrangements but placed parallel to each other and perpendicularly oriented to the diffusion direction, as shown in Fig. 10. The permeability in such a system is decreased due to the combined effects of the prolonged tortuous diffusion pathway and the reduced diffusion area. The relative permeability model and its tortuosity expression for random configurations of monodispersed flakes in composite systems are given as:

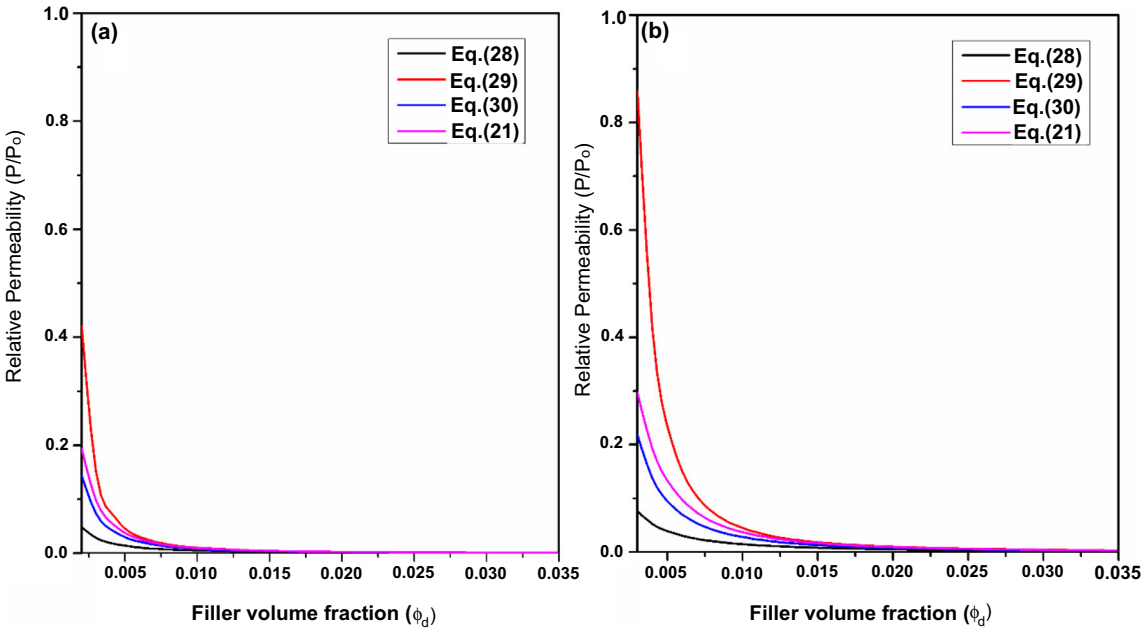

Fig. 9: Performance of tortuosity-based models for different filler aspect ratio (a) α=1000, σ =15, and (b) α=500, σ=15

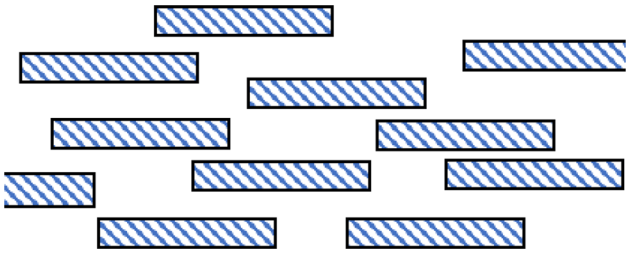

Fig. 10: Randomly oriented monodispersed flake-filled composite[60]

$$\frac{P}{P_o} = \frac{1-\phi_d}{\left(1+{}^{2}\!/_{3}\alpha\phi_d\right)^2}, \tag{33}$$

$$\tau = \left(1+{}^{2}\!/_{3}\alpha\phi_d\right)^2. \tag{34}$$

Guo et al.[62] derived an approximate tortuosity expression for randomly oriented and perpendicularly arrayed tubular fillers in a system of nanocomposite films comprising of poly(lactic acid) (PLA) and halloysite nanotubes (HNTs). Although an exact equation for the case shown in Fig. 11 is difficult to derive, an approximated expression describing the diffusion pathway around the tube is shown. The approximation considered appears to be elliptical rather than simply spherical or circular. Furthermore, it has been reported that fillers with tube shapes appear to have a smaller effect on the barrier performance even at higher loading. The corresponding expression for the tortuosity is:

$$\tau = 1 + \left(\frac{\pi^2-8}{16}\right)\phi_d, \tag{35}$$

While the relative oxygen permeability of the nanocomposite system with tubular fillers is described as:

$$\frac{P}{P_o} = \frac{1-\phi_d}{1+\left(\frac{\pi^2-8}{16}\right)\phi_d}. \tag{36}$$

In a system with tubular fillers, it can be noted that the model [equation (36)] is independent of aspect ratio (i.e., tube diameter and length) and the orientation of the fillers. Thus, the effectiveness of tubular fillers on the predicted barrier performance is significantly lower than that of the platelet fillers.

Cussler et al.[9] examined various cases of the formed slits among the randomly located parallel platelets of infinite length by introducing a combined geometric factor μ. This geometric factor characterizes the randomness of the system with porous media and increments the spacing between subsequent flake-platelets. The suggested expression for the prediction of relative permeability in composite films with the incorporation of the geometric factor is as follows:

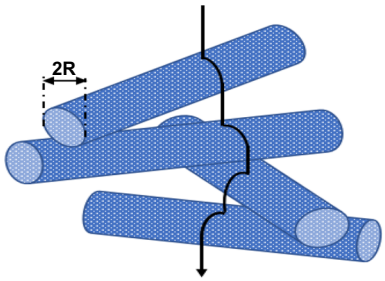

Fig. 11: Tubular or cylindrical fillers perpendicularly arrayed to gas diffusion direction[62]

$$\frac{P}{P_o} = \left(1+\frac{\mu\alpha^2\phi_d^2}{1-\phi_d}\right)^{-1}. \tag{37}$$

Effects of filler orientations

Bharadwaj[63] introduced orientation factor *S'* for different flake orientation angles. The factor ranges between −0.5 to 1. For handling a non-uniform orientation of platelets, the factor is defined to quantify the extent of flake orientation:

$$S' = \frac{1}{2}\langle 3\cos^2\theta - 1\rangle, \tag{38}$$

where θ is the angle between the penetrant flow direction and normal to the flake layer. Fig. 12 shows the elaboration of the orientation factor for different orientation angles. For a perfect alignment of platelets, i.e., θ = 0°, the orientation factor *S'* = 1, and for perpendicular or orthogonal orientation, i.e., θ = 90°, the factor *S'* = −0.5. The angular brackets in equation (38) denote to averaging for all platelets in the composite system. Moreover, the orientation factor *S'* = 0 corresponds to averaged angles of randomly distributed platelets or to platelets aligned with θ = 54.74°. The expression can also be used for different angles of the filler plates. For instance, for θ =30°, 45°, and 60°, the orientation factors are 0.625, 0.25, and −0.125, respectively.

Furthermore, Bharadwaj[63] modified the Nielsen model using the defined orientation factor *S'* for silicate fillers. The modification accounts for the effects of the clay filler orientations on the original tortuosity equation proposed by Nielsen [equation (16)]. The modified tortuosity expression containing the orientation factor is as follows:

$$\tau = 1 + \frac{L}{2W}\phi_d\left(\frac{2}{3}\right)\left(S' + \frac{1}{2}\right). \tag{39}$$

The relation equation (39) is mainly applied for a low loading of silicate layers, similar to what has been

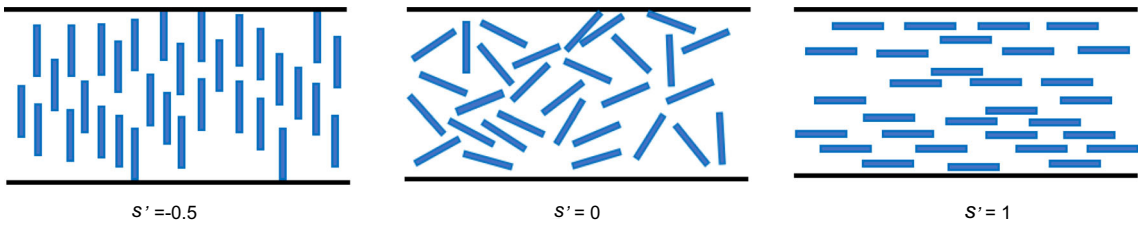

Fig. 12: Different possible cases of filler orientations in composite systems adapted by Bharadwaj[63]

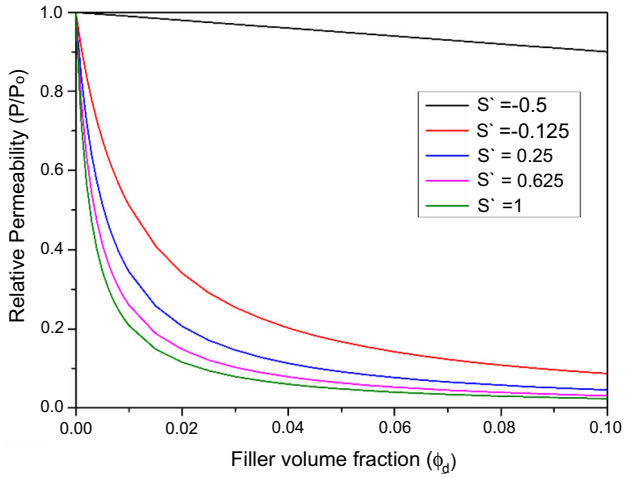

Fig. 13: Modified Nielsen model predictions for different orientation factors for α =750

defined for clay layers by Nielsen model [equation (17)]. However, for the case of higher silicate or clay flake loadings, stacking of layers is dominant in the composite system. Thus, to capture the morphological features of layer stacking, the extent or degree of stacking <N> is considered in the tortuosity equation, that is,

$$\tau = 1 + \frac{2}{3\langle N\rangle}\alpha\phi_d\left(S' + \frac{1}{2}\right). \tag{40}$$

Here, α is the aspect factor defined as L/W. For non-uniform orientations, the degree of orientation is taken as an average value, and uses the modified Nielsen model [equation (17)] with the orientation factor S' given by equation (38). The relative permeability can then be predicted using:

$$\frac{P}{P_o} = \frac{1-\phi_d}{1 + (\alpha/2)(2/3)(S' + 1/2)\phi_d}. \tag{41}$$

Figure 13 shows the modified Nielsen model [equation (41)] for different filler orientation/inclination angles θ ranging from 90° to 0° to the composite film surface. It can be seen that for a filler with a 90° inclination angle (i.e., orientation factor S' of −0.5), the contribution to barrier performance is minimum. The best enhancement is achieved when the inclination angle is zero ($S' = 1$) with respect to the film surface. For instance, with 10% filler loadings, the barrier enhancements for fillers inclination angle θ of 0°, 30°, 45°, 60°, and 90° are 97.66%, 96.91%, 95.44%, 94.59%, and 10%, respectively.

Nyflött et al.[64] modified Minelli's models [equations (30) and (31)] further by the introduction of orientation factor S' developed by Bharadwaj[63] and using a new control parameter for selecting the appropriate tortuosity regime in their composite system. The proposed tortuosity appears to be as follows:

$$\tau = \begin{cases} \dfrac{1}{2/3(S'+1/2)}\left[\dfrac{(\alpha\phi_d)^2(1+1/\alpha)^4}{1-\phi_d(1+1/\alpha)} + \dfrac{\alpha\phi_d}{\pi/4}(1+1/\alpha)^2\ln\left(\dfrac{1-\phi_d(1+1/\alpha)}{(\pi/2)\phi_d(1+1/\alpha)}\right)\right], r \le 1, \\ \dfrac{1}{2/3(S'+1/2)}\left[\alpha\phi_d + \dfrac{\alpha\phi_d}{\pi/4}(1+1/\alpha)^2\ln\left(\dfrac{\alpha(1+1/\alpha)}{\pi/2}\right)\right], r > 1, \end{cases} \tag{42}$$

In equation (42), the control parameter r which is used to distinguish between the tortuous regimes, is also modified. It is set to be:

$$r = \frac{\alpha - \alpha\phi_d}{\alpha^2\phi_d}. \tag{43}$$

Dondero et al.[65] modified Lape's tortuosity model by introducing the orientation factor described by Bharadwaj and by manipulating the factor 2/3 which accounts for the random dispersion of flakes in Lape Model [equation (33)]. The relative permeability equation with modified tortuosity expression proposed by Dondero et al.[65] reads as:

$$\frac{P}{P_o} = \frac{1-\phi_d}{[1 + (5/9)\alpha\phi_d(S' + 1/2)]^2}, \tag{44}$$

$$\tau = [1 + (5/9)\alpha\phi_d(S' + 1/2)]^2. \tag{45}$$

The model prediction exhibited a good agreement to the results obtained numerically using the boundary element method. For dilute and semi dilute or intermediate regimes, the model predictions were reported within an acceptable range of deviation (i.e., lower than 5%). However, for high loadings (i.e., for $\alpha\varphi_d$ 2), a maximum of 12% deviations were reported.

For a uniform distribution of flake orientations, Tsiantis and Papathanasiou[66] further modified Don-

dero model to capture the assumption of equal probability of random orientation in the interval of $-\pi\ /2\ <\ \theta\ >\ \pi/2$. Thus, for the case of uniform distribution of the flake orientations, the relative permeability equation is derived as:

$$\frac{P}{P_o} = \frac{1-\phi_d}{[1+(1+\sin(2\theta)/(2\theta))(5\alpha\phi_d/18)]^2}. \tag{46}$$

The tortuosity expression for the above modified Dondero model can be written as follows:

$$\tau = \left[1+\left(1+\frac{\sin(2\theta)}{2\theta}\right)\frac{5\alpha\phi_d}{18}\right]^2. \tag{47}$$

Sorrentino et al.[67] reported a different approach which led to the direct derivation describing the tortuosity factor in a heterogeneous system with inclined fillers, as shown in Fig. 14. The composite system geometry considered in their model includes flake length L, inter-flake spacing δ , thickness or slit depth t, slit gap ε and alignment angle θ.

The tortuosity expression obtained for the composite system shown in Fig. 14 can be presented as follows:

$$\tau = \left(\frac{L+2t}{L\sin\theta+2t\cos\theta}\right)^2. \tag{48}$$

Considering the system geometry shown in Fig. 14, if the fillers are parallel or perpendicular to the diffusion direction, i.e., inclination angle $\theta = \pi/2$ or 0°, then this leads to the cases of lowest (unity) and highest tortuosity values. The tortuosity expression in [equation (48)] becomes:

$$\tau = \begin{cases} (1+2t/L)^2 \cong 1, \theta = \pi/2 \\ (1+L/2t)^2, \theta = 0 \end{cases}. \tag{49}$$

Note that the Sorrentino model [equation (48)] is independent of the filler concentrations. Although it can be used for $\varphi_d >> 10\%$, but Sorrentino and his associates argued that equation (49) might not be valid for a lower filler concentration $\varphi_d << 10\%$ due to the fact that the free path in such dilute systems can be ignored. Therefore, for lower φ_d, Sorrentino et al.[67] proposed another tortuosity expression:

$$\tau = (1-\phi_d) + \phi_d\left(\frac{L+2t}{L\sin\theta+2t\cos\theta}\right)^2. \tag{50}$$

For dispersed fillers with randomly oriented flakes, an average of all the possible inclination angles θ is considered a representative of the composite system geometry. The orientation angle may range $(0 \le \theta \le \pi/2)$. The tortuosity expression for such randomly oriented composite is given as:

$$\tau = (1-\phi_d) + \phi_d\left[\frac{(L+2t)^2}{\pi Lt}\right]. \tag{51}$$

Using a similar approach as Sorrentino, Ly and Cheng[68] reported a different tortuosity model for a heterogeneous composite system containing impermeable fillers and organized in a regular array with variable orientation. The system geometry was defined via a filler width w, thickness λ, equal slit dimension and layer spacing δ, and orientation angle β. The aspect ratio ($\alpha = w/\lambda$) and slit/channel aspect ratio ($\sigma = \delta/\lambda$) were used for the model development (see Fig. 15). The tortuosity expression appears to be as follows

$$\tau = 6\left[\frac{16(1+\sigma)^2}{(\alpha+3\sigma+2)^2} + \frac{4(\alpha+\sigma)^2-8(1+\sigma)^2+8(\alpha+\sigma)(1+\sigma)}{(\alpha+3\sigma+2)^2}\sin^2\beta\right]^{-1}. \tag{52}$$

Equation (52) requires accurate values for w, λ and δ to provide the exact filler's aspect ratio, as well as the slit aspect ratio. However, it is difficult to measure these parameters experimentally if the system fillers are embedded within polymer nanocomposites.

Eitzman et al.[51] derived their expression for the calculation of the relative diffusivity of carbon dioxide

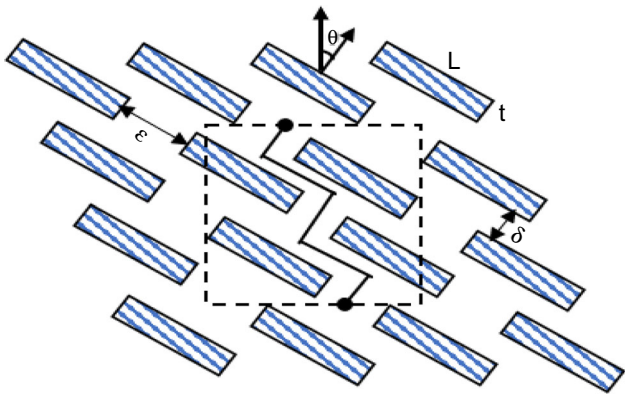

Fig. 14: Composite system with inclined fillers used for the calculation of tortuosity factor by Sorrentino et al.[67]

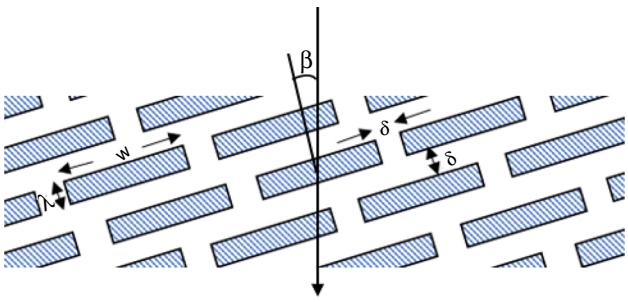

Fig. 15: Composite system with inclined domains/fillers with angle β[68]

through silicone-polycarbonate films with oriented mica flakes. According to their expression for tipped flakes, the available diffusion area reduction was compensated through the introduction of a squared cosine of the tipped angle θ on the second term of Cussler's model [equation (26)], which corresponds to the tortuous pathway. The tortuosity equation used in their work is:

$$\tau = \frac{\alpha^2 \phi_d^2}{1 - \phi_d} \cos^2 \theta. \tag{53}$$

Tsiantis and Papathanasiou[69] proposed a model which is capable of reproducing accurately computational results. The proposed model combines the Lape model [equation (33)] and Nielsen model [equation (17)] with modifications accounting for randomly placed flakes' orientation angle. The model is capable of dealing in systems of aspect ratio α ranging 100-1000, and range of regimes varying from dilute ($\alpha\varphi_d = 0.01$) to concentrated ($\alpha\varphi_d = 40$) regimes. According to the expression given for the relative diffusivity, their relative permeability equation is.

$$\frac{P}{P_o} = (1 - \phi_d)\left[\frac{1}{(1 + \alpha\phi_d/\lambda)^2}\cos^2\theta + \frac{1}{(1 + \phi_d/2\alpha)}\sin^2\theta\right]. \tag{54}$$

Similarly, the tortuosity model used in combination with Lape and Nielsen tortuosity equations [equations (34) and (16)] with flake orientation angle θ takes the form;

$$\tau = \left[\frac{1}{(1 + \alpha\phi_d/\lambda)^2}\cos^2\theta + \frac{1}{(1 + \phi_d/2\alpha)}\sin^2\theta\right]^{-1}, \tag{55}$$

where λ is a geometric parameter, which can be adjusted to different values to represent the actual length of a pathway traveled by the diffusion gas molecule. λ was given as 3 in Lape model [equation (33)], which assumes that the diffusion path around the flake is a straight line.

Effects of filler stacking

Brydges et al.[70] employed a new parameter known as the stacking parameter (γ), which is defined as $\gamma = x/2d$, where the parameter is always less than unity ($\gamma < 1$). The parameter is to describe the exact location of the ribbon-like parallel platelets. This parameter is indicative of deviation from the regular interval of platelets, which is defined by the horizontal offset of each ribbon layer in relation to the layer below it. The value $\gamma = 1/2$ gives the lowest permeability, which corresponds to the case when the ribbons are arranged as brick and mortar style, i.e., when a ribbon in the first layer centered over the gap/slit of the layer beneath (see Fig. 8). However, if $\gamma = 0$, then a maximum increase in permeability will be obtained. Brydges et al.[70] modified Cussler's model with the factor $\gamma(1-\gamma)$. For high aspect ratio ($\alpha = 2d/a > 100$) and equivalent slit dimension with its depth ($2s \approx$ a), the tortuosity expression and the corresponding permeation model are as follows:

$$\tau = 1 + \frac{\alpha^2 \phi_d^2}{1 - \phi_d}\gamma(1 - \gamma), \tag{56}$$

$$\frac{P}{P_o} = \left(1 + \frac{\alpha^2 \phi_d^2}{1 - \phi_d}\gamma(1 - \gamma)\right)^{-1}. \tag{57}$$

Further, Nazarenko et al.[71] modified the Nielsen model to account for the case of stacking of layers, i.e., agglomerates, which are dispersed homogenously and oriented perpendicularly to the direction of diffusion. The following expression was proposed:

$$\frac{P}{P_o} = \frac{1 - \phi_d}{1 + \left(\frac{1}{3}\right)\frac{\alpha}{2N}\phi_d}. \tag{58}$$

The tortuosity equation used in this case appears to be similar to that of the Nielsen model, which can be expressed as:

$$\tau = 1 + \left(\frac{1}{3}\right)\frac{\alpha}{2N}\phi_d, \tag{59}$$

where N is the number of layers in the layer stacks, if $N = 1$ signifies to the complete layer exfoliation (delamination). If the value of N is high, then the enhancement of barrier properties tends to deteriorate.

Effects of filler regimes

Fredrickson and Bicerano [72] have employed a second-order approximation using scattering theory to formulate their model. The approach characterizes dilute and semi-dilute regimes in composite systems, as shown in Fig. 16. The relative permeability equation used in the Fredrickson and Bicerano model can be rearranged in a general form as[73, 74]:

$$\frac{P}{P_o} = \frac{(1 - \phi_d)}{4[(1 + x + 0.1245x^2)/(2 + x)]^2}, \tag{60}$$

where $x = \pi\alpha\varphi_d/[2\ln(\alpha/2)]$. The corresponding tortuosity expression for Fredrickson and Bicerano model as reported in the literature[75] is:

$$\tau = 4\left[\frac{(1 + x + 0.1245x^2)}{(2 + x)}\right]^2. \tag{61}$$

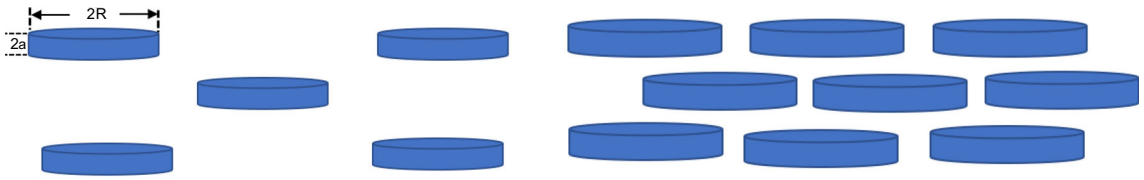

Fig. 16: Dilute and a semi-dilute regime of circular disc fillers adapted by Fredrickson and Bicerano[72]

Furthermore, Sun et al.[74] validated the Fredrickson and Bicerano model [equation (60)] using experimental relative permeability results obtained for nanocomposite films comprising epoxy and synthetic α-zirconium phosphate platelets (epoxy/ZrP nanocomposite films). According to Sun et al.,[74] the Fredrickson and Bicerano model predictions showed a good fit with the experimental results.

Fredrickson and Bicerano[72] investigated the two cases of impermeable circular disc platelets with radius R, thickness $2a$, and the aspect ratio $\alpha = R/2a$. For the case of the dilute regime of disc-filled composite (Fig. 16 a), the discs were spaced by a distance more than the disc radius R. A similar expression to Nielsen's model tortuosity expression [equation (16)] was derived, namely:

$$\tau = 1 + \kappa\alpha\phi_d, \tag{62}$$

where $\kappa = \pi/ln\alpha$. This case corresponds to the dilute regime with a low volume fraction of the filler and aspect ratio ($\alpha\varphi_d << 1$). However, for semi-dilute regimes (Fig. 16b), the low volume fraction of the filler, but high aspect ratio value (i.e., $\alpha\varphi_d >> 1$), the disc overlaps, and the expression for the tortuosity becomes:

$$\tau = 1 + \mu\alpha^2\phi_d^2, \tag{63}$$

where $\mu = \pi^2/16\ln 2\alpha$. The expression appears to be similar to the expression reported in equation (21) by Cussler et al.[9] Using a different approach, Gusev and Lusti[76] developed a 3D computational model for a system with a random array of parallelly aligned circular discs. The expression for the relative permeability prediction given in their case is:

$$\frac{P}{P_o} = \frac{1-\phi_d}{\exp\left[-(\alpha\phi_d/x_o)^{\beta}\right]}, \tag{64}$$

$$\tau = e^{-\left(\frac{\alpha\phi_d}{x_o}\right)^{\beta}}, \tag{65}$$

where β and x_o are constant parameters of 0.71 and 3.47, respectively. Picard et al.[77] used the same constants to obtain similar results to Nielsen's model prediction in nylon-6/montmorillonite composites.

Effects of fillers polydispersity

Picard et al.[77] modified the model reported by Lape et al.[61] considering the polydispersity of filler width and thickness. The suggested modified model is given as follows:

$$\frac{P}{P_o} = \frac{1-\phi_d}{\left[1 + (1/3)\phi_d \sum n_i(w_i/t_i)^2 \Big/ \sum n_i(w_i/t_i)\right]^2}. \tag{66}$$

The tortuosity equation for the system of polydisperse fillers with varying width and thickness appears to be a modified form of the Lape model, which considers the actual thickness of tactoids and the distribution of the aspect ratio values. The proposed tortuosity expression can be put as:

$$\tau = \left[1 + (1/3)\phi_d \sum n_i(w_i/t_i)^2 \Big/ \sum n_i(w_i/t_i)\right]^2, \tag{67}$$

where w_i and t_i are the width and thickness of the platelet i, respectively. The above model is appropriate for higher loading of impermeable fillers with agglomerates and distribution of aspect ratio within the composite system.

It is clear that various tortuosity-based models have been developed and modified to capture the composite system's morphological features. Initially, the models were developed for simplified ideal geometries. However, it is practically difficult to obtain a composite system with fillers perfectly aligned, equally spaced, parallelly oriented, and completely exfoliated clay layers. Although these morphological features of the composite are unlikely to be achieved, however, such ideal filler geometries were considered as the main assumptions during model development in most cases. Consequently, various researchers modified the tortuosity-based models to describe their composite systems. Thus, the resulting models are specific to a

particular composite system. Hence, the developed or modified models may not be relevant to other composite systems with different morphological features. Hence, the experimental validation of models with different composite system remains a challenge. Therefore, a case-to-case investigation of the modified models may not result in accurate predictions since there is always a variation in system morphological features such as clay orientations, alignment, polydispersity (variable aspect ratio), distribution (variable slit factor), etc. Hence, models with better prediction accuracy for a particular polymer–particle composite system may not produce similar prediction accuracy for other composites.

Moreover, the variation in polymer–clay pairs also adds to the complexity as their interactions directly impact composite film fabrication. For example, it is challenging to control the clay orientation in polymer composites or avoid stacking clay layers experimentally. No universal tortuosity-based model was developed to describe the complexity of the composite system with irregular filler geometries. In most cases, researchers simplify their system to fit particular model predictions, and accordingly, either modification is suggested or performed if the deviations are considerable.

The following research gaps can be highlighted regarding the tortuosity model development for barrier applications.

1. Composite systems are heterogeneous with a variety of filler geometries, sizes and properties; expressing such systems mathematically to determine the tortuous pathway precisely remains challenging.
2. Composite films with nanofillers composed of nanoplatelets and nanoparticles usually form entwined nano-channels, such channels appear to be networks of free particles which connect the nanoblocks, which seem to have more tortuous pathways for the diffusing gas.[27] Such systems tortuous pathways remain unmodeled.
3. The comparison of predicted results with experimental values is usually carried out with rough estimations, lacking a quantified value of errors in terms of absolute average relative errors or standard deviations. Hence, it becomes difficult for the reader to identify the most accurate tortuosity-based models.
4. To date, there is no model developed that represents fillers of combined filler shapes within a single composite system. In some practical cases, researchers incorporated spherical filler in addition to flake-shaped platelets to reduce the slit area. Many other filler shapes can also be added depending on the target application of the barrier material. The tortuosity expression in such cases remains unmodeled.

Conclusions

Impermeable inclusions in a polymer coating film result in improved gas barrier properties owing to the prolonged diffusion pathways followed by the penetrant gas molecules. Modeling the gas barrier properties performances of coating films is crucial to determine the preservation and shelf-life of food in packaging prior to the coating film preparation. Modeling approaches employed for barrier materials mainly focus on identifying and characterizing the tortuosity factor for the composite system. Hence, several tortuosity-based models have been proposed depending on the system morphological features. Most of the existing tortuosity-based models are phenomenological. They work well for simplified geometries of inclusions like fillers with identical shapes, regular geometries, parallel alignment to the film surface, perfectly oriented, and well-dispersed across the coating film volume. Moreover, to reflect the heterogeneity in the composite system, progressive modifications were performed by several researchers. This review only focused on analytical tortuosity models developed for gas barrier applications. Other approaches like those fitting to porous media are not included here. We, therefore, recommend that the modeling of such composite systems should exploit the knowledge of the changes induced due to filler inclusions on the polymer properties such as free-volume change, polymer–particle interphase, and other relevant system parameters.

Acknowledgment The authors would like to acknowledge the financial support obtained from KK Foundation Karlstad University and the industry partners in the Multi-Barr synergy project:-Iggesund Paperboard AB, Cellcomb AB, OMYA, and UMV.

Funding Open access funding provided by Karlstad University.

References

1. Rhim, J-W, Park, H-M, Ha, C-S, ''Bio-nanocomposites for food packaging applications.'' *Progress in Polymer Science*, **38** (10–11) 1629–1652 (2013)
2. Su, Y, Kravets, VG, Wong, SL, Waters, J, Geim, AK, Nair, RR, ''Impermeable barrier films and protective coatings based on reduced graphene oxide.'' *Nature Communications*, **5** 4843 (2014)
3. Blanchard, A, Gouanvé, F, Espuche, E, ''Effect of humidity on mechanical, thermal and barrier properties of EVOH films.'' *Journal of Membrane Science*, **540** 1–9 (2017)
4. Mangaraj, S, Yadav, A, Bal, LM, Dash, SK, Mahanti, NK, ''Application of biodegradable polymers in food packaging industry: A comprehensive review.'' *Journal of Packaging Technology and Research*, **3** (1) 77–96 (2018)
5. FAO, ''Food wastage footprint: Impacts on natural sources—Summary report.'' p. 63. Food and Agriculture Organization of the United Nations, Rome, Italy (2013)
6. Barlow, CY, Morgan, DC, ''Polymer film packaging for food: an environmental assessment.'' *Resources, Conservation, and Recycling*, **78** 74–80 (2013)
7. Johansson, C, Bras, J, Mondragon, I, Nechita, P, Plackett, D, Simon, P, Svetec, DG, Virtanen, S, Baschetti, MG, Breen, C, Aucejo, S, ''Renewable fibers and bio-based materials for packaging applications: a review of recent developments.'' *Bioresources*, **7** 2506–2552 (2012)
8. Olsson, E, Johansson, C, Järnström, L, ''Montmorillonite for starch-based barrier dispersion coating—Part 1: The influence of citric acid and poly(ethylene glycol) on viscosity and barrier properties.'' *Applied Clay Science*, **97–98** 160–166 (2014)
9. Cussler, EL, Hughes, SE, Ward, WJ, Aris, R, ''Barrier membranes.'' *Journal of Membrane Science*, **38** (2) 161–174 (1988)
10. Cui, Y and Kumar, S, ''Improving Gas Barrier Performance of Polymer Nanocomposites with Carbon Nanotube Nanofillers.'' *ECS Meeting Abstracts*, 1064 (2016)
11. Liu, M, Jia, Z, Jia, D, Zhou, C, ''Recent advance in research on halloysite nanotubes-polymer nanocomposite.'' *Progress in Polymer Science*, **39** (8) 1498–1525 (2014)
12. Introzzi, L, Blomfeldt, TO, Trabattoni, S, Tavazzi, S, Santo, N, Schiraldi, A, Piergiovanni, L, Farris, S, ''Ultrasound-assisted pullulan/montmorillonite bionanocomposite coating with high oxygen barrier properties.'' *Langmuir*, **28** (30) 11206–11214 (2012)
13. Dunkerley, E, Schmidt, D, ''Effects of composition, orientation and temperature on the O_2 permeability of model polymer/clay nanocomposites.'' *Macromolecules*, **43** (24) 10536–10544 (2010)
14. Nyflött, Å, Moons, E, Bonnerup, C, Carlsson, G, Järnström, L, Lestelius, M, ''The influence of clay orientation and crystallinity on oxygen permeation in dispersion barrier coatings.'' *Applied Clay Science*, **126** 17–24 (2016)
15. Bhunia, K, Dhawan, S, Sablani, SS, ''Modeling the oxygen diffusion of nanocomposite-based food packaging films.'' *Journal of Food Science*, **77** (7) N29–N38 (2012)
16. Mittal, V, ''Modelling and prediction of barrier properties of polymer layered silicate nanocomposites.'' *Polymers & Polymer Composites*, **21** (8) 509–517 (2013)
17. Loryuenyong, V, Saewong, C, Aranchaiya, C, Buasri, A, ''The improvement in mechanical and barrier properties of poly(vinyl alcohol)/graphene oxide packaging films.'' *Packaging Technology and Science*, **28** (11) 939–947 (2015)
18. Noshirvani, N, Ghanbarzadeh, B, Fasihi, H, Almasi, H, ''Starch–PVA nanocomposite film incorporated with cellulose nanocrystals and MMT: A comparative study.'' *International Journal of Food Engineering*, **12** (1) 37–48 (2016)
19. Cairns, MJ, Mesic, B, Johnston, JH, Herzog, MB, ''Use of spherical silica particles to improve the barrier performance of coated paper.'' *Nordic Pulp & Paper Research Journal*, **34** (3) 334–342 (2019)
20. Cairns, MJ, Mesic, B, Johnston, JH, Hill, SJ, Kirby, N, ''Tetraethylorthosilicate-containing barrier dispersion coatings—Mechanism of action.'' *Progress in Organic Coatings*, **139** 105443 (2020)
21. Wijmans, JG, Baker, RW, ''The solution-diffusion model: a review.'' *Journal of Membrane Science*, **107** (1–2) 1–21 (1995)
22. Wijmans, JG and Baker, RW, ''The solution–diffusion model: A unified approach to membrane permeation.'' In: Y. Yampolskii, Pinnau, I and Freeman, BD (eds.) *Materials Science of Membranes for Gas and Vapor Separation*, pp. 159-189. John Wiley and Sons, Chichester, West Sussex, England (2006)
23. Klopffer, MH, Flaconneche, B, ''Transport properties of gases in polymers: Bibliographic review.'' *Oil & Gas Science and Technology*, **56** (3) 223–244 (2001)
24. Flaconneche, B, Martin, J, Klopffer, MH, ''Transport properties of gases in polymers: Experimental methods.'' *Oil & Gas Science and Technology*, **56** (3) 245–259 (2006)
25. Stenqvist, B, Sparr, E, ''Tortuosity in the brick and mortar model based on chemical conduction.'' *Chemical Engineering Science*, **223** 115729 (2020)
26. Carrera, MC, Erdmann, E, Destéfanis, HA, ''Barrier properties and structural study of nanocomposite of HDPE/montmorillonite modified with polyvinylalcohol.'' *Journal of Chemistry*, **2013** 1–7 (2013)
27. Bhattacharya, M, Biswas, S, Bhowmick, AK, ''Permeation characteristics and modeling of barrier properties of multifunctional rubber nanocomposites.'' *Polymer*, **52** (7) 1562–1576 (2011)
28. Martinez-Hermosilla, GA, Mesic, BB, Bronlund, JE, ''A review of thermoplastic composites vapour permeability models: Applicability for barrier dispersion coatings.'' *Packaging Technology and Science*, **28** (7) 565–578 (2015)
29. Tan, B, Thomas, NL, ''Tortuosity model to predict the combined effects of crystallinity and nano-sized clay mineral on the water vapour barrier properties of polylactic acid.'' *Applied Clay Science*, **141** 46–54 (2017)
30. Maxwell, JC, *A Treatise on Electricity and Magnetism*. Clarendon Press, London (1881)
31. Zid, S, Zinet, M, Espuche, E, ''Modeling diffusion mass transport in multiphase polymer systems for gas barrier applications: A review.'' *Journal of Polymer Science Part B: Polymer Physics*, **56** (8) 621–639 (2018)
32. Rayleigh, L, ''LVI. On the influence of obstacles arranged in rectangular order upon the properties of a medium.'' *The London, Edinburgh, and Dublin Philosophical Magazine and Journal of Science*, **34** (211) 481–502 (1892)
33. Bruggeman, DAG, ''Berechnung verschiedener physikalischer Konstanten von heterogenen Substanzen. I. Dielektrizitätskonstanten und Leitfähigkeiten der Mischkörper aus isotropen Substanzen.'' *Annalen der Physik*, **416** (7) 636–664 (1935)
34. Idris, A, Man, Z, Maulud, AS, Uddin, F, ''Modified Bruggeman models for prediction of CO_2 permeance in polycarbonate/silica nanocomposite membranes.'' *The Canadian Journal of Chemical Engineering*, **95** (12) 2398–2409 (2017)

35. Shariati, A, Omidkhah, M, Pedram, MZ, ''New permeation models for nanocomposite polymeric membranes filled with nonporous particles.'' *Chemical Engineering Research and Design*, **90** (4) 563–575 (2012)
36. Xia, X, Zhong, Z, Weng, GJ, ''Maxwell–Wagner–Sillars mechanism in the frequency dependence of electrical conductivity and dielectric permittivity of graphene-polymer nanocomposites.'' *Mechanics of Materials*, **109** 42–50 (2017)
37. Bouma, RHB, Checchetti, A, Chidichimo, G, Drioli, E, ''Permeation through a heterogeneous membrane: The effect of the dispersed phase.'' *Journal of Membrane Science*, **128** (2) 141–149 (1997)
38. Rafiq, S, Maulud, A, Man, Z, Mutalib, MIA, Ahmad, F, Khan, AU, Khan, AL, Ghauri, M, Muhammad, N, ''Modelling in mixed matrix membranes for gas separation.'' *The Canadian Journal of Chemical Engineering*, **93** (1) 88–95 (2015)
39. Nielsen, LE, ''Models for the permeability of filled polymer systems.'' *Journal of Macromolecular Science: Part A - Chemistry*, **1** (5) 929–942 (1967)
40. DeRocher, J, Gettelfinger, B, Wang, J, Nuxoll, E, Cussler, E, ''Barrier membranes with different sizes of aligned flakes.'' *Journal of Membrane Science*, **254** (1–2) 21–30 (2005)
41. Xu, B, Zheng, Q, Song, Y, Shangguan, Y, ''Calculating barrier properties of polymer/clay nanocomposites: Effects of clay layers.'' *Polymer*, **47** (8) 2904–2910 (2006)
42. Bharadwaj, RK, Mehrabi, AR, Hamilton, C, Trujillo, C, Murga, M, Fan, R, Chavira, A, Thompson, AK, ''Structure–property relationships in cross-linked polyester–clay nanocomposites.'' *Polymer*, **43** (13) 3699–3705 (2002)
43. Kojima, Y, Fukumori, K, Usuki, A, Okada, A, Kurauchi, T, ''Gas permeabilities in rubber-clay hybrid.'' *Journal of Materials Science Letters*, **12** (12) 889–890 (1993)
44. Sheng, N, Boyce, MC, Parks, DM, Rutledge, GC, Abes, JI, Cohen, RE, ''Multiscale micromechanical modeling of polymer/clay nanocomposites and the effective clay particle.'' *Polymer*, **45** (2) 487–506 (2004)
45. Abdullah, ZW, Dong, Y, Han, N, Liu, S, ''Water and gas barrier properties of polyvinyl alcohol (PVA)/starch (ST)/glycerol (GL)/halloysite nanotube (HNT) bionanocomposite films: Experimental characterisation and modelling approach.'' *Composites Part B: Engineering*, **174** (107033) 1–10 (2019)
46. Huang, H-D, Ren, P-G, Chen, J, Zhang, W-Q, Ji, X, Li, Z-M, ''High barrier graphene oxide nanosheet/poly(vinyl alcohol) nanocomposite films.'' *Journal of Membrane Science*, **409–410** 156–163 (2012)
47. Yang, C, Smyrl, WH, Cussler, EL, ''Flake alignment in composite coatings.'' *Journal of Membrane Science*, **231** (1–2) 1–12 (2004)
48. Moggridge, GD, Lape, NK, Yang, C, Cussler, EL, ''Barrier films using flakes and reactive additives.'' *Progress in Organic Coatings*, **46** (4) 231–240 (2003)
49. Cui, Y, Kumar, S, Rao Kona, B, van Houcke, D, ''Gas barrier properties of polymer/clay nanocomposites.'' *RSC Advances*, **5** (78) 63669–63690 (2015)
50. Wakeham, WA, Mason, EA, ''Diffusion through multiperforate laminae.'' *Industrial & Engineering Chemistry Fundamentals*, **18** (4) 301–305 (1979)
51. Eitzman, DM, Melkote, RR, Cussler, EL, ''Barrier membranes with tipped impermeable flakes.'' *Aiche Journal*, **42** (1) 2–9 (1996)
52. Perry, D, Ward, WJ, Cussler, EL, ''Unsteady diffusion in barrier membranes.'' *Journal of Membrane Science*, **44** (2–3) 305–311 (1989)
53. Aris, R, ''On the permeability of membranes with parallel, but interconnected, pathways.'' *Mathematical Biosciences*, **77** (1–2) 5–16 (1985)
54. Aris, R, ''On a problem in hindered diffusion.'' *Archive for Rational Mechanics and Analysis*, **95** (2) 83–91 (1986)
55. Falla, WR, Mulski, M, Cussler, EL, ''Estimating diffusion through flake-filled membranes.'' *Journal of Membrane Science*, **119** (1) 129–138 (1996)
56. Swannack, C, Cox, C, Liakos, A, Hirt, D, ''A three-dimensional simulation of barrier properties of nanocomposite films.'' *Journal of Membrane Science*, **263** (1–2) 47–56 (2005)
57. Goodyer, CE, Bunge, AL, ''Comparison of numerical simulations of barrier membranes with impermeable flakes.'' *Journal of Membrane Science*, **329** (1–2) 209–218 (2009)
58. Minelli, M, Baschetti, MG, Doghieri, F, ''Analysis of modeling results for barrier properties in ordered nanocomposite systems.'' *Journal of Membrane Science*, **327** (1–2) 208–215 (2009)
59. Minelli, M, Baschetti, MG, Doghieri, F, ''A comprehensive model for mass transport properties in nanocomposites.'' *Journal of Membrane Science*, **381** (1–2) 10–20 (2011)
60. Lape, NK, Yang, CF, Cussler, EL, ''Flake-filled reactive membranes.'' *Journal of Membrane Science*, **209** (1) 271–282 (2002)
61. Lape, NK, Nuxoll, EE, Cussler, EL, ''Polydisperse flakes in barrier films.'' *Journal of Membrane Science*, **236** (1–2) 29–37 (2004)
62. Guo, Y, Yang, K, Zuo, X, Xue, Y, Marmorat, C, Liu, Y, Chang, C-C, Rafailovich, MH, ''Effects of clay platelets and natural nanotubes on mechanical properties and gas permeability of poly (lactic acid) nanocomposites.'' *Polymer*, **83** 246–259 (2016)
63. Bharadwaj, RK, ''Modeling the barrier properties of polymer-layered silicate nanocomposites.'' *Macromolecules*, **34** (26) 9189–9192 (2001)
64. Nyflött, Å, Petkova-Olsson, Y, Moons, E, Bonnerup, C, Järnström, L, Carlsson, G, Lestelius, MM, Minelli, M, ''Modeling of oxygen permeation through filled polymeric layers for barrier coatings.'' *Journal of Applied Polymer Science* (2017). https://doi.org/10.1002/app.44834
65. Dondero, M, Tomba, JP, Cisilino, AP, ''The effect of flake orientational order on the permeability of barrier membranes: Numerical simulations and predictive models.'' *Journal of Membrane Science*, **514** 95–104 (2016)
66. Tsiantis, A, Papathanasiou, TD, ''A closed-form solution for the barrier properties of randomly oriented high aspect ratio flake composites.'' *Journal of Composite Materials*, **53** (16) 2239–2247 (2019)
67. Sorrentino, A, Tortora, M, Vittoria, V, ''Diffusion behavior in polymer-clay nanocomposites.'' *Journal of Polymer Science Part B: Polymer Physics*, **44** (2) 265–274 (2006)
68. Ly, YP, Cheng, Y-L, ''Diffusion in heterogeneous media containing impermeable domains arranged in parallel arrays of variable orientation.'' *Journal of Membrane Science*, **133** (2) 207–215 (1997)
69. Tsiantis, A, Papathanasiou, TD, ''The barrier properties of flake-filled composites with precise control of flake orientation.'' *Materials Sciences and Applications*, **08** (03) 234–246 (2017)
70. Brydges, WT, Gulati, ST, Baum, G, ''Permeability of glass ribbon-reinforced composites.'' *Journal of Material Science*, **10** 2044–2049 (1975)
71. Nazarenko, S, Meneghetti, P, Julmon, P, Olson, BG, Qutubuddin, S, ''Gas barrier of polystyrene montmorillonite clay nanocomposites: Effect of mineral layer aggregation.''

Journal of Polymer Science Part B: Polymer Physics, **45** (13) 1733–1753 (2007)
72. Fredrickson, GH, Bicerano, J, ''Barrier properties of oriented disk composites.'' *The Journal of Chemical Physics*, **110** (4) 2181–2188 (1999)
73. Takahashi, S, Goldberg, HA, Feeney, CA, Karim, DP, Farrell, M, O'Leary, K, Paul, DR, ''Gas barrier properties of butyl rubber/vermiculite nanocomposite coatings.'' *Polymer*, **47** (9) 3083–3093 (2006)
74. Sun, L, Boo, WJ, Clearfield, A, Sue, HJ, Pham, HQ, ''Barrier properties of model epoxy nanocomposites.'' *Journal of Membrane Science*, **318** (1–2) 129–136 (2008)
75. Cui, Y, Kundalwal, SI, Kumar, S, ''Gas barrier performance of graphene/polymer nanocomposites.'' *Carbon*, **98** 313–333 (2016)
76. Gusev, AA, Lusti, HR, ''Rational design of nanocomposites for barrier applications.'' *Advanced Materials*, **13** (21) 1641–1643 (2001)
77. Picard, E, Vermogen, A, Gerard, J, Espuche, E, ''Barrier properties of nylon 6-montmorillonite nanocomposite membranes prepared by melt blending: Influence of the clay content and dispersion state consequences on modelling.'' *Journal of Membrane Science*, **292** (1–2) 133–144 (2007)